

Seasonal stabilization effects slowed the greening of the Northern Hemisphere over the last two decades

Received: 10 July 2024

Accepted: 19 June 2025

Published online: 08 July 2025



Wen Zhang¹✉, William K. Smith¹, Trevor F. Keenan^{2,3},
Matthew P. Dannenberg⁴, Yang Li¹, Songhan Wang⁵, John S. Kimball⁶ &
David J. P. Moore¹✉

Rising atmospheric CO₂ and warming spring temperatures increase vegetation growth and the terrestrial carbon sink. However, drought, heat stress, phenology, and resource limitations may stabilize or limit these projected increases. We investigate the balance between these amplifying and stabilizing ecological factors by asking whether enhanced early-season growth leads to continued late-season growth. Using the Moderate Resolution Imaging Spectroradiometer (MODIS) leaf area index (LAI) dataset, we identify three seasonal growth patterns based on early- and peak-season positive LAI anomalies: (1) amplification, where late-season LAI anomalies exceed earlier ones; (2) weak stabilization, where late-season anomalies remain similar or slightly lower; and (3) strong stabilization, where late-season anomalies become negative. Weak and strong stabilization events dominate across 67% and 26% of Northern Hemisphere ecosystems above 30°N, respectively. The absence of any trend in amplifying or stabilizing events suggests stabilizing factors seasonally offset CO₂ and temperature-induced spring greening. Terrestrial biosphere models underestimate strong stabilization and overestimate amplification events. This inconsistency arises from the models' underestimation late-season LAI sensitivity to precipitation in water-limited regions; overlook negative legacy effects of early enhanced LAI on late-season soil moisture via evapotranspiration losses in energy-limited regions. Our findings suggest water/heat stress and resource limitations limit greening and the land carbon sink.

The seasonality of vegetation activities in the Northern Hemisphere (NH) is critical to the global carbon cycle^{1,2}. As temperature rises, advances in the timing of spring green-up have been documented globally across hundreds of plant species^{3–6}. High atmospheric CO₂ concentrations stimulate plant growth across a wide range of

ecosystems^{7–10}, and enhanced greening at global scales is often attributed to rising CO₂^{11,12}. Early and peak season greening can increase the land carbon sink^{13,14} unless it is offset by reductions in carbon uptake later in the growing season^{15–18}. Evaluating the connection from early and peak-season to late-season growth—specifically,

¹School of Natural Resources and the Environment, University of Arizona, Tucson, AZ, USA. ²Department of Environmental Science, Policy, and Management, UC Berkeley, Berkeley, CA 94720, USA. ³Climate and Ecosystem Sciences Division, Lawrence Berkeley National Laboratory, Berkeley, CA 94720, USA. ⁴School of Earth, Environment, and Sustainability, University of Iowa, Iowa City, IA, USA. ⁵Jiangsu Collaborative Innovation Center for Modern Crop Production/Key Laboratory of Crop Physiology and Ecology in Southern China, College of Agriculture, Nanjing Agricultural University, Nanjing, China. ⁶NTSG, University of Montana, Missoula, MT, USA. ✉e-mail: wenzhang1@arizona.edu; davidjpmoore@arizona.edu

the persistence of early growth enhancement into the late season—offers a valuable opportunity to determine whether growth-amplifying factors are strengthened or stabilized by growth-limiting factors.

Enhanced early and peak-season growth may enable more growth later in the season (amplification), or late-season growth may be limited by lack of resources or life history limitations (stabilization), and there is prior evidence for both amplification and stabilization effects. For grasses, shrubs, and some trees, amplification may occur by a ‘carry over effect’, where more leaf area early in the season leads to higher light absorption which in turn enhances late season greenness and vegetation productivity^{19–21} (Fig. 1). Anomalies of early season LAI may also be maintained in the late season through simple persistence or delayed senescence of LAI²². In contrast, early growth may increase water and nutrient resource demand which limits late season vegetation growth^{19,23–25}. For example, greater transpiration can lead to soil moisture depletion and thus limit late season plant growth. Late season biophysical stressors such as drought and heatwave events may also limit late season vegetation growth^{26,27}. Thus, comparing observations of early- and peak-season LAI anomalies to late- season LAI anomalies is a measure of the balance of factors that amplify growth and factors that stabilize growth. This allows us to evaluate whether models can capture this balance correctly.

Long-term, sub-seasonal observations of LAI provide an opportunity to investigate these complex seasonal trajectories and their temporal evolution over the past twenty years. Previously, research has relied on joining partially overlapping remote sensing estimates of leaf area index (LAI) from a variety of sensors²⁴. However, these datasets have some limitations, including issues with sensor calibration, satellite drift, atmospheric correction, and data fusion resulting in inconclusive findings^{28,29}. These issues can be avoided by analyzing LAI estimates from the twin Moderate Resolution Imaging Spectroradiometer (MODIS) sensors. The MODIS LAI observations provide meticulously validated and collaboratively developed datasets, ensuring consistent sensor performance and careful consideration of uncertainties related to atmospheric correction and sensor degradation^{30,31}. The MODIS sensor record now spans more than twenty years, providing an opportunity for reliable and comprehensive assessments of seasonal greenness trajectories and model evaluations

without the risk of bias introduced by fusion of multiple sensor records^{32,33}.

In this study, we use the latest Collection 6 MODIS LAI/FPAR product (MCD15A2H v006^{31,34}) to compare the strength and direction of early- and peak-, and late-season LAI anomalies. In addition, we also use the AVHRR LAI3g product²⁸ and global eddy covariance (EC) GPP estimates³⁵. To test whether growth amplifying factors outweigh growth stabilizing factors, we focus our analysis on all occurrences of positive LAI anomalies in the early- and peak- growing season (see “Methods”) and compare them to the magnitude of late-season LAI anomalies. We next quantify the spatial distribution and temporal frequency of three types of scenarios: 1) amplification, where positive late-season LAI anomalies exceed early- and peak-season LAI anomalies; 2) weak stabilization, with late-season LAI anomalies equal to or less than those of earlier seasons; and 3) strong stabilization, where negative late-season LAI anomalies follow positive early- and peak-season anomalies (see “Methods”). We identify key drivers of these scenarios using high resolution climate data, including precipitation and temperature estimates from the Climatic Research Unit (CRU³⁶) and soil moisture estimates from the Global Land Evaporation Amsterdam Model (GLEAM v3a³⁷). To evaluate whether widely used terrestrial biosphere models (TBMs) faithfully represent enhanced seasonal growth extending from early and peak seasons to late season, we compare our MODIS and AVHRR LAI3g anomaly estimates to LAI simulations from TBMs that participate in the TRENDY Version 11 (TRENDYv11³⁸) intercomparison project (Supplementary Table 1). Our main objectives are to: 1) examine the spatial variation and temporal changes of seasonal LAI trajectory scenarios; 2) explore the mechanisms controlling the balance of amplifying and stabilizing effects in different ecosystems; and 3) quantify TBM skill in reproducing observed seasonal LAI trajectories, their sensitivity to climate, and legacy effects from vegetation-soil feedbacks.

Results and discussion

Stabilization has been dominant in the past two decades

Enhancement of early- and peak- season LAI did not lead to widespread enhancement of late season LAI. Across the 19-year MODIS record, the percentage of occurrence of each scenario across all events was strongly biased toward stabilizing scenarios (Fig. 2a).

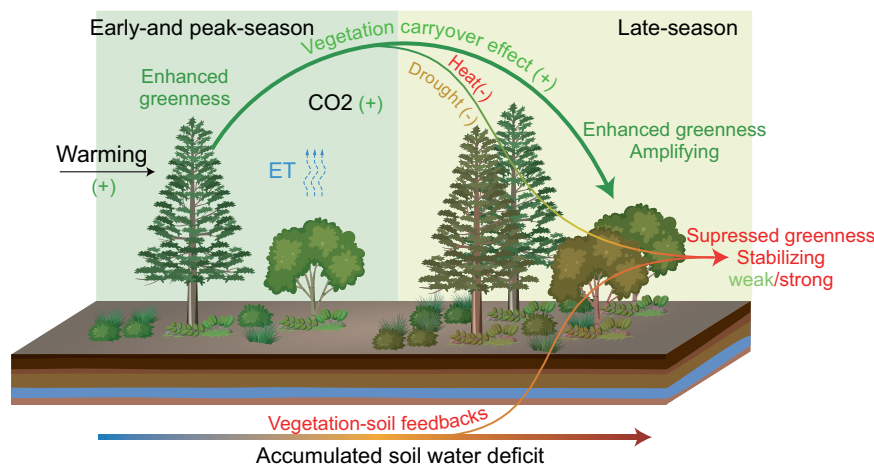


Fig. 1 | Schematic representation of the seasonal greenness trajectory scenarios that capture the strength and directions from enhanced early- and peak-season greenness to late-season greenness. Warming and CO₂ stimulate enhanced vegetation greenness during the early- and peak- growing season, which can persist into the late growing season through amplifying effects (green line). Alternatively, the increased greenness observed in the early and peak seasons could be inhibited or even reversed in the late season (weak/strong stabilization scenarios, indicated by the orange line). This may result from intrinsic phenological

and life history limitations, seasonal climate anomalies, or accumulated soil moisture deficits caused by the intensified greenness in the early-and peak-seasons, which could deplete soil moisture due to enhanced evapotranspiration (ET). The symbols – and + in each bracket represent either a negative or positive effect, respectively, on terrestrial vegetation greenness. Trees icons were designed by and sourced from Vecteezy.com under a Free License: <https://www.vecteezy.com/vector-art/8334831-isolated-trees-and-nature-objects-set> zheli.

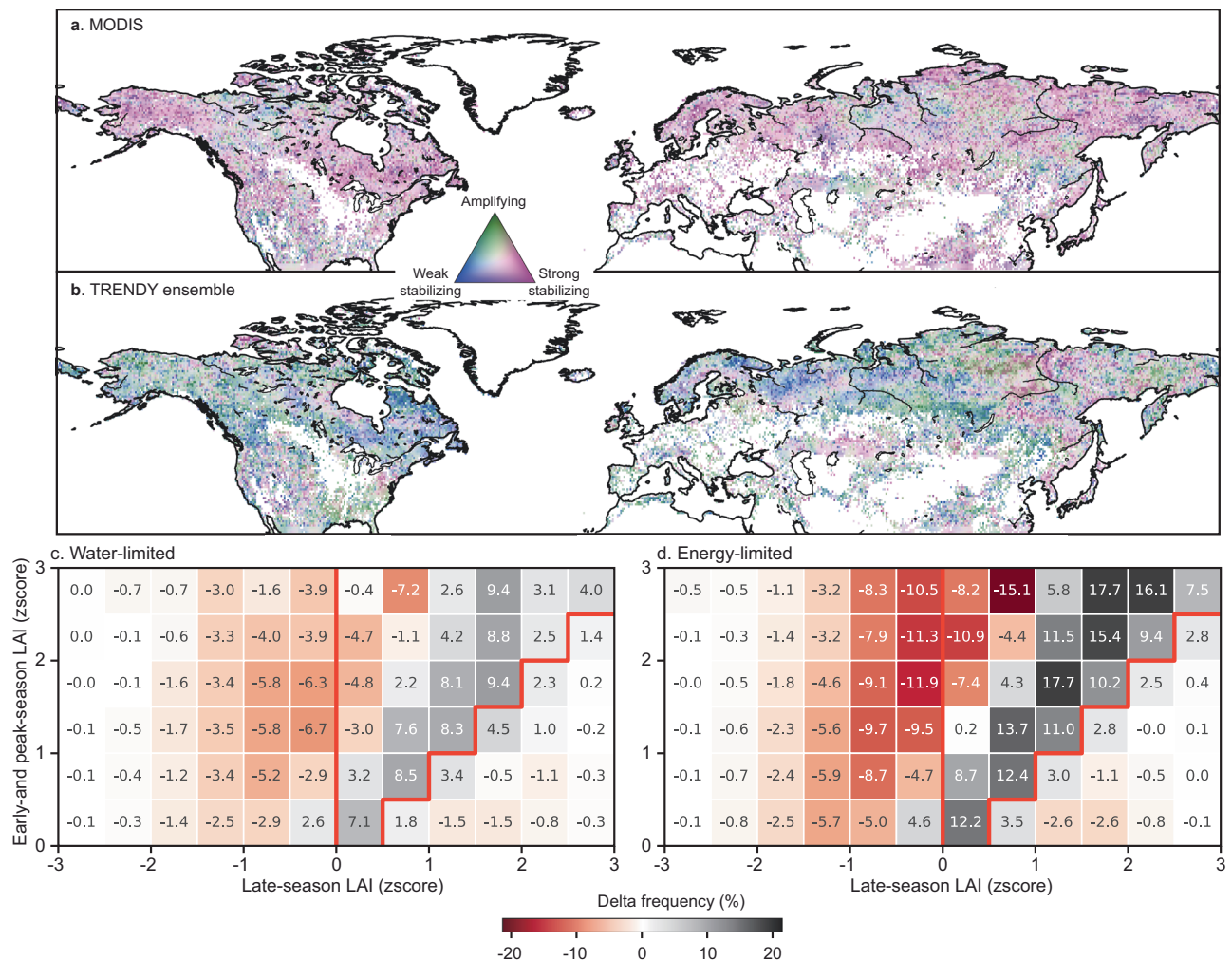


Fig. 2 | Observed dominance of stabilization events in the Northern Hemisphere is largely underestimated by models. The probability of dominant event (strong stabilization: pink, weak stabilization: blue, and amplification: green) for MODIS (a) and TRENDY ensemble (b), respectively. Each pixel is a composite of these three scenarios, with the colors representing the probability for each scenario within that pixel. The colors are calculated by assigning a magenta-blue-green value to each grid depending on the percentage of occurrence of each scenario across all analyzed events. The matrix presents the differences between TRENDY and MODIS. We show the difference in the percentage of occurrences for strong stabilization (where late-season LAI z-score < 0), weak stabilization (where late-season LAI z-score > 0 but lower than early- and peak-season LAI), and amplification (where late-season LAI z-score exceeds early- and peak-season LAI) for water-limited (c) and energy-limited regions (d), (see Methods). The staircase line in the matrix represents a 1:1 reference line, indicating points where late-season LAI anomalies are equal to early- and peak-season LAI anomalies. Data points on this line implies

that the late-season growth matches the early- and peak-season growth. The right side of the staircase line shows conditions where late-season LAI is greater than early- and peak-season LAI, indicating amplification. Conversely, the left side of the staircase line represents cases where late-season LAI is smaller than early- and peak-season LAI, indicating stabilization. The color intensity represents the magnitude of the difference in occurrence probability between TRENDY and MODIS. Greyish hues indicate that TRENDY ensemble overestimates the probability relative to MODIS, while reddish hues indicate underestimation. Only scenarios with a positive z-score for early- and peak-season LAI are considered. Areas that were cultivated, managed, or non-vegetated are excluded from the analysis and represented in grey. All maps use the linear convolution interpolation method. Supplementary Fig. 5 shows the same map without interpolation. Map of panel a and b generated with python 3-mpltoolkits.basemap(version 1.4.1, <https://matplotlib.org/basemap/stable/>).

Weak and strong stabilization dominant events were more prevalent (occurring in more than 51% of years) than amplification dominant events over 93% of the Northern Hemisphere. Strong stabilization dominant events alone were prevalent across 26% of locations studied. Widespread stabilization dominant events could be explained by internal or external limits to plant growth or feedbacks caused by the increased demand for resources required by greater early- and peak- season leaf area. In contrast, amplification dominant events were prevalent across only 7% of the Northern Hemisphere. Our findings suggest that benefits into the late season are modest, despite previous report showing positive correlations between early-, peak- and late-season vegetation productivity²⁰. These patterns were similar in other datasets, with seasonal stabilization also

dominant in AVHRR LAI3g observations (Supplementary Fig. 1). We found stabilization effects were broadly consistent across all plant functional types whether they exhibited evergreen or deciduous growth habits (Supplementary Fig. 2). Grassland contributed an increasing percentage of high probability under weak stabilization and a decreasing percentage under strong stabilization. While the resolution of the datasets we use may blend signals from the understory and herbaceous in evergreen systems³⁹, optical remote sensing has proven to be highly effective in detecting physical and biological changes in evergreen vegetation activity and photosynthesis⁴⁰. Considering the significant role that deciduous forests play in the NH carbon sink^{41,42}, especially given the recent shifts where deciduous forests are increasingly replacing evergreen

forests due to disturbances such as fire⁴³, further investigation using higher-resolution datasets is needed.

When analyzed identically, models within the TRENDY ensemble consistently underestimated the LAI stabilization dominant events compared to observation-based estimates. In the Northern Hemisphere, the TRENDY ensemble depicted strong and weak stabilization dominant events in total across 81% of regions (Fig. 2b). The dominance of strong stabilization was especially underestimated, comprising only 5% of Northern Hemisphere land area (compared to MODIS observations of 26%). Significant underestimation of strong stabilization effects was observed across large regions, covering 75% of the study area, with underestimations reaching up to 80%. This contributed to the model's inability to accurately capture strong dominant events (Supplementary Fig. 3). Conversely, the TRENDY ensemble tended to significantly overestimate amplification dominant events compared to MODIS observations. Specifically, more than 19% of areas exhibited amplification dominance in the TRENDY ensemble (compared to MODIS observations of 7%). Across individual model, amplification dominant events were overestimated in 5 out of the 9 TRENDY models, while only 2 demonstrated widespread stabilization (Supplementary Fig. 4).

Model significantly underestimated strong stabilization events across all cases

We further explored how varying levels of late-season greenness correspond to different magnitudes of positive early- and peak- season LAI anomalies (see Supplementary Fig. 6). Widespread strong stabilization was found across all early- and peak-season LAI positive anomaly events, with consistent patterns observed in MODIS, AVHRR LAI3g (Supplementary Fig. 7), and GPP observations (Supplementary Fig. 8). Across the 27 available flux tower sites, seasonal stabilization of GPP was more common than seasonal amplification, occurring at 69% of the sites. The differences between TRENDY and MODIS metrics showed that TRENDY tended to underestimate the occurrence of strong stabilization effects in nearly all cases during early- and peak-season LAI increase events (where early- and peak-season LAI z-scores > 0). This underestimation was present in both water-limited and energy-limited regions (Fig. 2c, d). In weak stabilization events, the models exhibited biases based on the strength of the late-season response. Specifically, the models underestimated stronger weakening effects (e.g., where the late-season z-score ranges from 0.5 to 1). In contrast, the models overestimated weaker weakening effects (e.g., where the late-season z-score was greater than 1). The models tended to overestimate amplification events when its magnitude was low, while underestimating in the rare cases when amplification was high.

Climatic drivers and vegetation-soil moisture feedbacks influence seasonal LAI trajectory in different ecosystems

Our findings suggest that water availability controls whether early LAI enhancement persists into the late season and that this is controlled by *water input* in water limited systems and *water consumption* in energy limited systems. Structural equation modeling (SEM; see methods) indicated that early- and peak-season LAI responses to water and temperature were consistent with expected ecological sensitivity to limiting factors across the Northern Hemisphere: early- and peak-season LAI were mostly influenced by precipitation in water-limited systems but temperature in energy-limited systems. Peak season precipitation appeared to influence LAI in the late season indirectly through an apparent effect on late season soil moisture (SM) everywhere (Fig. 3a, d), but the positive effect of precipitation on SM was 5 times greater in water-limited systems than energy-limited systems (slope 4.062 vs 0.738, Fig. 3a, d). Early- and peak-season LAI anomalies in water limited systems did not lead to enhanced late season LAI when early gains were not accompanied by sufficient precipitation (i.e. negative peak-season precipitation anomalies; Fig. 3b). These patterns

are supported by observations from site level, remote sensing and experiments in dryland where late season plant phenology and greenness is strongly dependent on precipitation inputs^{44–48}.

In contrast, in energy limited systems we saw little evidence that water inputs vary between amplification and stabilization (Fig. 3e, f). Instead, positive early- and peak- season LAI anomalies combined with nearly simultaneous positive temperature anomalies likely caused greater SM to dry down in the late season. Positive early- and peak-season LAI anomalies tended to decrease the amount of SM available in the late season in both water-limited and energy-limited regions, but this negative effect was larger in energy limited systems (-0.718 vs -0.458 ; Fig. 3a, d), most likely because energy limited systems maintain higher LAI, are more productive, and use more water in absolute terms. This suggested feedback is supported by previous findings that enhanced early- and peak-season LAI increases evapotranspiration (ET), leading to excessive soil moisture depletion and subsequently limiting vegetation growth in the late season^{19,23–25}. We did observe an 'enhanced peak season ET' under strong stabilization scenarios in both water-limited and energy-limited regions (Supplementary Fig. 9a, c). Positive LAI anomalies during the early- and peak- seasons significantly increased ET in both regions, with a greater effect observed in water-limited areas compared to energy-limited regions (0.504 vs. 0.349; Supplementary Fig. 9b, d). This increase in ET further depleted late-season soil moisture, with a particularly pronounced impact in energy-limited systems than water-limited regions (-0.435 vs. -0.004). Grasslands are highly responsive to both seasonal climatic variability and resource limitations such as water and nutrients availability⁴⁹ and so may respond to short term resource availability^{50–52}. Experimental warming-induced depletion of soil moisture may lead to reductions in late-season LAI or accelerated autumn leaf senescence in temperate grassland⁵³ and arctic plants⁵⁴, but temperate forest species show little experimental response⁵³. On a larger scale, an analysis of tree diameter growth across 108 forests in Eastern North America found that earlier onset of spring growth caused by natural variation in temperature, did not translate into enhanced annual growth because of summer or late season growth limitations⁵⁵. These phenomena may be because earlier spring phenology in temperate regions may result in earlier leaf senescence, limiting increases in late-season LAI^{56–58}. Warm spring temperatures can lead to early snow melt, enhanced carbon uptake during spring and summer and late season water deficits^{17,59} which could explain enhanced spring growth and late season water limitation in evergreen forests dependent on snow. Water stress and high temperatures can significantly limit nutrient mineralization as during periods of drought or elevated temperatures, microbial activity declines more sharply due to reduced soil moisture and heat stress on microbial communities, resulting in a marked reduction in nutrient availability^{60,61}.

Terrestrial biosphere models failed to capture impacts of climate factors and complex vegetation-soil moisture feedback on late season LAI

Terrestrial Biosphere Models (TBMs) failed to describe how water availability controls persistence of early LAI enhancement into the late season, resulting in underestimates of stabilization effects throughout the northern hemisphere. In water limited regions, the controls of precipitation input on late season LAI were accurately modeled (b path 8), but models varied widely in their estimate of the effect of peak season precipitation input on late season SM. In energy limited regions, seven of nine of the models did not accurately replicate the effect of water consumption use on late season SM, instead showing a less negative or sometimes positive effect of early- and peak-season LAI on late season SM (Fig. 4c, path 3). The observations suggested that high temperatures in the late season dry out late season SM, but the models significantly underestimated the negative relationships between late-season temperatures and

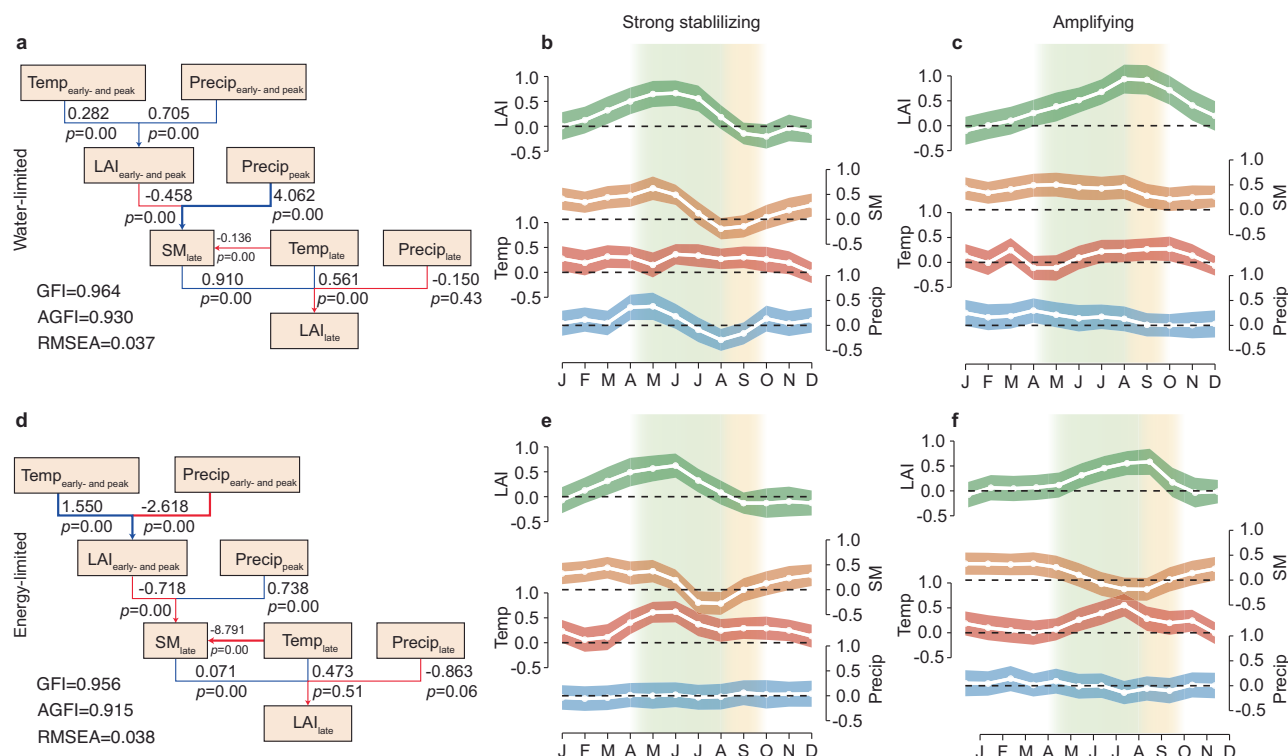


Fig. 3 | Factors controlling seasonal LAI trajectories from early- and peak-season LAI to late season LAI. Causality networks illustrating the factors influencing seasonal LAI dynamics among environmental factors and vegetation-soil feedback as deduced from structural equation models (SEMs) for water-limited (a) and energy-limited regions (d). Red lines indicate negative effects and blue lines indicate positive effects, while line thickness is proportional to the strength of the relationship and to the standard path coefficients adjacent to each line. The goodness-of-fit index (GFI), adjusted goodness-of-fit index (AGFI), and root mean square error of approximation (RMSEA) are labeled alongside each response variable in the model. The mean seasonal LAI and hydroclimatic variables, aggregated

across both time and space, are shown separately for water-limited (b) and energy-limited (e) regions under strong stabilization, as well as for water-limited (c) and energy-limited (f) regions under amplification scenarios, respectively. The hydroclimatic variables depicted include soil moisture (SM), temperature (Temp), and precipitation (Precip), all displayed as monthly z-scores relative to the study period mean (2003–2021). Sample size are 34198 in water-limited region and 113202 in energy-limited region. The shaded areas represent ± 0.5 standard deviations. A two-sided t test was used to assess the significance of the path coefficients of SEM analysis. Multiple comparisons are not applicable.

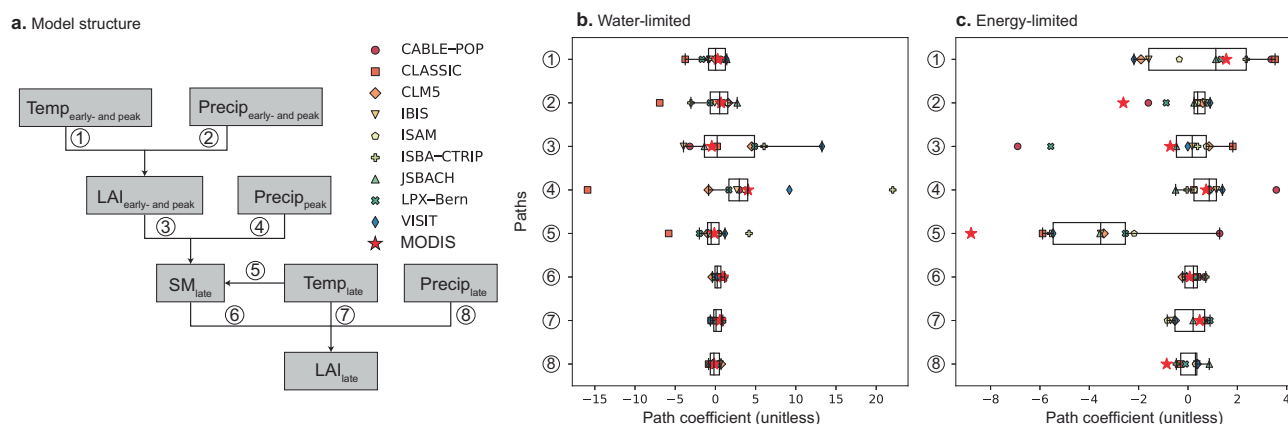


Fig. 4 | Observed versus modeled mechanisms linking early- and peak-season LAI to late-season LAI. The comparison of path coefficient of SEM (a) between MODIS and individual TRENDY models for (b) water-limited regions and (c) energy-limited regions. Precipitation and temperature data were obtained from CRU

records, the same forcing data used for TRENDYv11, while soil moisture was derived from the respective outputs of individual models. Boxplots from left to right represent minimum, first quartile, median, third quartile and maximum values, with sample size of 10.

late-season soil moisture (Fig. 4a, c, path 5, Supplementary Fig. 10). The combined errors in vegetation-SM feedbacks (path 3) and lower temperature-driven evapotranspiration (path 5) would overestimate SM in the late season and may explain why TBMs fail to show stabilization of early- and peak-season LAI anomalies into the late season. These mechanisms may explain some of the modelled

overestimation of the land carbon sink^{62–64}. This explanation is supported by previous analyses that these TBMs failed to accurately estimate vegetation-soil feedbacks, misrepresented leaf senescence, and had unrealistic climate sensitivities^{20,38}.

Failure to correctly represent factors that stabilize positive early- and peak- season LAI anomalies can increase errors in model estimates

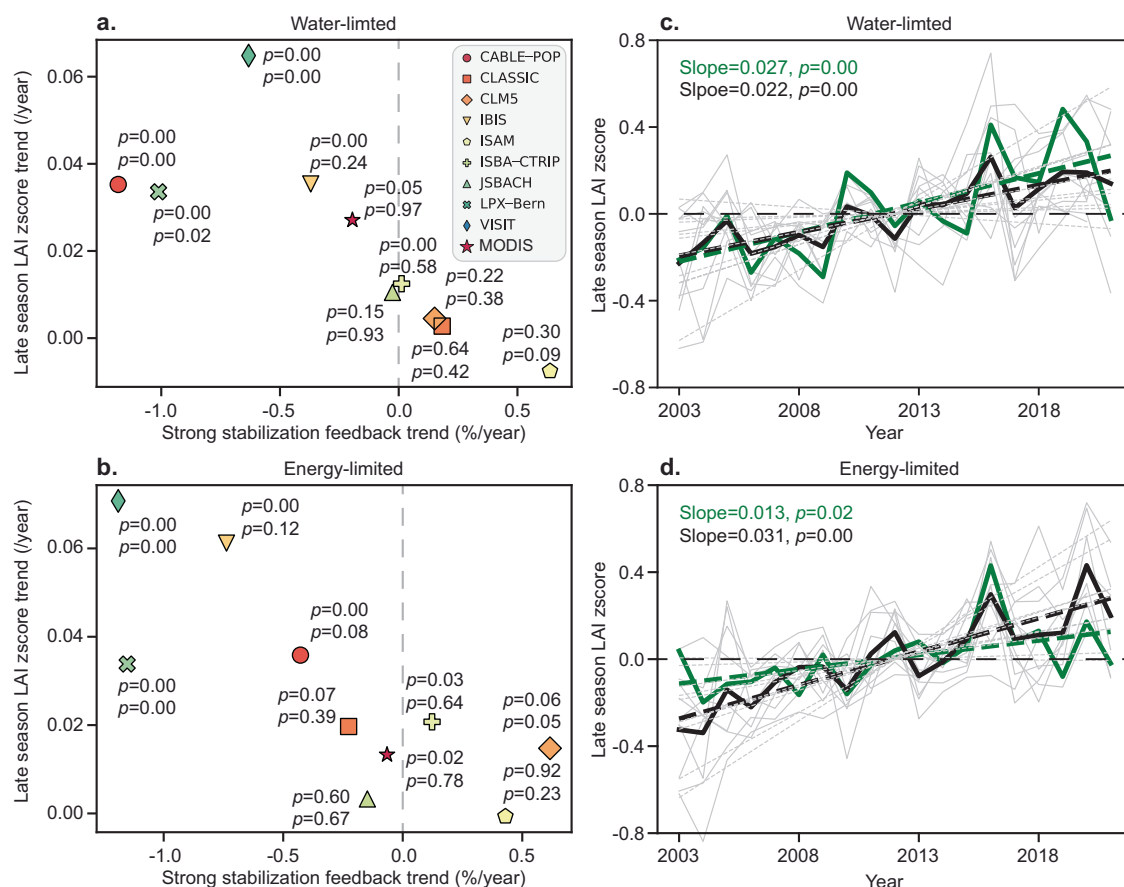


Fig. 5 | Observed versus modeled trends in strong stabilization events and late-season LAI. The relationship between trends in the frequency of strong stabilization events and in late-season LAI among MODIS observation and individual models from 2003 to 2021 for both water-limited (**a**) and energy-limited (**b**) regions. Time series of the averaged late-season LAI for the water-limited (**c**) and energy-limited (**d**) regions among MODIS (green color) and TRENDY ensemble (black color) and all

individual model (grey color). The p values (p) in (**a**) and (**b**) for the trends in late-season LAI are presented above, while those for the strong stabilizing feedbacks are provided below. Sample size is 34198 in water-limited region and 113202 in energy-limited region. The significance level was evaluated using a two-sided t test on the basis of ordinary least squares regression model.

of vegetation growth through time. Vegetation growth is controlled by many factors, and some would be expected to influence the observed patterns of amplification or stabilization that we have described in terms of temperature and moisture controls only. CO₂ fertilization tends to increase both LAI and water-use efficiency^{8,9,65,66}, and late season LAI could be enhanced through delayed leaf senescence mediated by warm temperatures^{14,67}. Given the apparent sensitivity of late season LAI to water availability, we would expect rising temperature and CO₂ to manifest in our analysis as fewer instances of strong stabilization of late-season LAI through time. Despite the well documented increase in mean global temperature and drought occurrence^{68,69}, we were unable to detect a change in the frequency of stabilization or amplification events over two decades. Observations showed no evidence of any trend in late-season LAI stabilization (Fig. 5a, b, $P=0.97$ for water-limited region and $P=0.78$ for energy-limited regions). However, a recent analysis of SIF and NDVI spanning nearly four decades documented a shift from less stabilization of early season productivity enhancements into summer productivity to more stabilization with the increased frequency of adverse summer moisture conditions¹⁹. Trends in late-season LAI stabilization differ among TRENDY models, though many individual models show disagreement with observations. Notably, 6 out of 9 models predicted widespread greening, leading to an overestimation of late-season greening trends compared to actual observations. Some individual models, such as CABLE-POP and VISIT, exaggerated these trends even further, significantly overestimating late-season LAI increases (Supplementary

Fig. 11). Both IBIS and VISIT showed declines in strong stabilization events in water- and energy-limited systems (Fig. 5a, b). While LPX-Bern showed significantly more stabilization events than other models (Supplementary Fig. 4h), there was a detectable decrease in the frequency of these events through time in both water-limited (Fig. 5a, $P=0.02$) and energy-limited regions (Fig. 5b, $P=0.00$). Strong stabilization events increased in CLM simulations, which could result from inaccuracies in leaf phenology sensitivity to environmental change⁷⁰. JSBACH agreed with the observed patterns in the frequency of stabilization events and accurately captured the direction and magnitude of LAI responses to precipitation and temperature as well as vegetation-soil moisture feedback throughout the entire season (Supplementary Fig. 4g, Supplementary Fig. 10). The process errors that lead to less stabilization of early season enhancements (Fig. 5a, b) would tend to overestimate LAI and could explain part of the consistent LAI bias in TBMs^{71,72} and Earth System models^{73,74}. The patterns observed in the ensemble mute the biases in many of the models. The balance of these model responses led the TRENDY ensemble to predict a similar, though slightly greater overall increase in late-season LAI compared to observations in energy-limited region (Fig. 5c, d, Supplementary Fig. 12b, d).

Across the northern hemisphere and throughout the last two decades, the magnitude of late-season LAI enhancement was less than that of early- and peak-season LAI (Supplementary Fig. 12a–d). Models overestimate the positive influence of factors that should result in enhanced late season LAI and underestimate factors that constrain

late-season LAI. Our analysis suggests that some models could be improved by more appropriately characterizing constraints and feedbacks mediated by water input and water consumption. However, trends in late-season LAI could also be influenced by changes in vegetation structure and composition⁷⁵, nutrient constraints^{76,77}, sink limitations^{78,79}, and climatic patterns⁸⁰ that cannot be fully disentangled in our analysis.

We found that early enhancements in LAI observed in the last two decades frequently do not persist to the late growing season across the northern hemisphere. The greater the enhancement in early- and peak-season LAI was, the less likely it was to carry over into the late season, which implicates resource use limitation. Our findings suggest that widespread stabilization is mediated by the lack of water input in water-limited systems and excessive water consumption in energy-limited systems. Accurately representing the balance of amplifying and stabilizing factors in models is important to predicting the future carbon sink strength of the Northern Hemisphere. However, we found that the most recent collection of TRENDY models (v11) often underestimated the occurrence of stabilization events compared to satellite observations. If, as suggested by our analysis, moisture controls are responsible for the widespread stabilization of early season LAI enhancement, we expect these stabilization factors to become more important in future. Considering the projected increase in the frequency and severity of future heat/drought events in some regions of the Northern Hemisphere in the 21st century^{69,81}, our analysis suggests further divergence between satellite and model LAI estimates and potential negative consequences for the projected global land carbon sink.

Methods

Satellite-based LAI products. We used the 8-day, 500-meter resolution Moderate Resolution Imaging Spectroradiometer (MODIS) Collection 6 (C6) LAI products (MCD15A2H), including both the Terra and Aqua MODIS LAI products (MOD15A2H and MYD15A2H), covering the period 2003–2021. The 8-day LAI were aggregated to monthly scale using the Maximum Value Composite method⁸². For comparison, we also used an updated version of Advanced Very High-Resolution Radiometer (AVHRR) LAI3g product covering the period 1982–2018²⁸. This AVHRR LAI3g dataset is available at 8-km spatial resolution and biweekly temporal resolution⁸³. To create the AVHRR LAI3g dataset, an artificial neural network algorithm was used to train the overlapping data (2000–2016) from the Global Inventory Modeling and Mapping Studies (GIMMS) NDVI3gV1⁸⁴ and C6 Terra MODIS LAI datasets. Similarly, the biweekly AVHRR LAI3g were aggregated to monthly scale. The high-resolution satellite data was then aggregated to a 0.5° spatial grid by averaging all cells that fall within 0.5° cell to match the resolution of the temperature and precipitation data.

Eddy covariance (EC) measurements

To independently verify the remote sensing analyses, we conducted additional analyses using daily Gross Primary Production (GPP) estimates from FLUXNET2015³⁵. The FLUXNET2015 database includes 177 sites in the northern hemisphere representing 13 major vegetation types based on the classification system of the International Geosphere Biosphere Programme (IGBP⁸⁵). For our analysis, we selected sites that had a minimum of 5 years of records after 2003 and excluded agricultural sites, leaving a total of 27 northern sites (>30°N; Supplementary Table 2). We excluded early- to peak-season negative GPP z-scores (see Methods Early- to peak- season and late season extraction).

TRENDYv11 models

We used monthly LAI simulation outputs for 2003–2021 from 9 process-based terrestrial biosphere models participating in the TRENDY (trends in net land–atmosphere carbon exchange) v6

project³⁸: CABLE-POP, CLASSIC, CLM5, IBIS, ISAM, ISBA-CTRIP, JSBACH, LPX-Bern and VISIT (details in Supplementary Table 1). All models performed the same set of factorial simulations following a standard experimental protocol⁸⁶. Here, we used TRENDY simulation S2 that was forced by varying both atmospheric CO₂ and climate. The LAI simulations from TRENDYv11, ranging in spatial resolution from 0.5° to 2° (Supplementary Table 1), were resampled to a common 0.5° grid using the nearest neighbor method to ensure the model outputs were comparable with the satellite data. In addition to the LAI simulations, we also used monthly soil moisture outputs from the same 9 process-based terrestrial biosphere models in the TRENDY v6 project, which provided consistent soil moisture data over the period 2003–2021. The soil moisture outputs were extracted from the TRENDY S2 simulation, which, like the LAI data, was driven by both varying atmospheric CO₂ and climate conditions. To ensure comparability with observational datasets, the SM outputs were also resampled to a common 0.5° grid using the nearest neighbor method. These SM outputs were then incorporated into our analysis to investigate the relationships between early- and peak-season LAI anomalies and their effects on late-season soil moisture dynamics.

Climatic and soil moisture

We used gridded (0.5° resolution) monthly time series of temperature and precipitation from the Climatic Research Unit (CRU) v4.0.1 dataset³⁶, the same forcing data used for TRENDYv11. The Global Land Evaporation Amsterdam Model (GLEAM) v3.2a³⁷ of root soil moisture with a spatial resolution of 0.25° over the period of 2003–2021 was used to represent soil moisture (SM). Subsequently, we transformed the SM from a 0.25° resolution to 0.5° by averaging the values of the four 0.25-degree cells within each 0.5-degree cell. This adjustment was made to ensure alignment with the resolution of the temperature and precipitation data.

MCD12Q1 land cover data

We obtained annual land cover from the MODIS 500-m land cover product (MCD12Q1 v006), spanning from 2003 to 2021, using the 17-class International Geosphere-Biosphere Program (IGBP) classification scheme^{85,87}. To eliminate the impact of land cover changes, we excluded pixels that underwent substantial land cover change during the study period. Specifically, we calculated the proportion of each vegetation type from all 500-meter pixels falling within each 0.5° grid cell and computed the trends of each vegetation type based on the full 2003–2020 time series. The net change was calculated by multiplying the trends by the length of the years. If the net change for any vegetation type exceeded 10% within a given 0.5° pixel, we considered that pixel to have experienced significant land cover change and removed it from the analysis. We also excluded any 0.5° pixels over 60% of areas dominated by cultivated, managed, or non-vegetated land.

Early-, peak-, and late-season definition

To estimate seasonal trajectories between early- and peak- season LAI and late-season LAI, we divided the mean seasonal cycle of LAI (based on the 19-year study period) into early-, peak-, and late-season periods for each grid cell. We first smoothed the LAI curves of the three LAI products (MODIS, AVHRR LAI3g, and TRENDY v11) for each year using the Harmonic Analysis of NDVI Time Series (HANTS) algorithm^{88–90}. This algorithm uses a Fourier transform to remove pronounced outliers in a time series and reconstruct a smooth curve⁸⁹. We then used threshold-based method to retrieve the start and end of the growing season (SOS and EOS, respectively). SOS and EOS were defined as follows: SOS occurs when the LAI for a given pixel first exceeds 20% above the annual minimum LAI for that pixel. EOS occurs when the LAI declines to 20% above the annual minimum value. The early growing season was further defined as the period from SOS to the date when LAI reaches 50% of its annual maximum. The late growing season was

defined as the period from the date LAI reaches 50% of its maximum to the EOS. The peak growing season was defined as the period between the early and late growing seasons (Supplementary Fig. 13). We then combined the early and peak seasons, referring to them collectively as the early- and peak-season. We used the same approach to define early-, peak-, and late-season GPP at the EC sites. We excluded grid cells that had their maximum LAI before April or after October and pixels with multiple LAI peaks within a year. Since we focus on interseasonal mean vegetation growth states (LAI) instead of the shift of phenological events, we used the multiyear-averaged smoothed LAI to determine the early, peak, and late seasons.

We detrend the vegetation data (LAI and GPP) for each month before analyzing the seasonal dynamics. This approach allowed us to focus specifically on the seasonal component, ensuring that any long-term trends did not obscure the seasonal patterns of interest. By detrending each month, we were able to isolate intra-annual variability, which was crucial for understanding the seasonal relationships in the LAI data. For consistency, we applied the same detrending method to the environmental drivers as well. This ensured that both vegetation indices and environmental variables were analyzed on an equivalent basis, thereby reducing the risk of overstating the sensitivity estimates due to remaining long-term trends in the environmental data.

Water- and energy-limited regions

We classified regions as either water or energy limited (Supplementary Fig. 14) using the aridity index, calculated as the ratio of annual precipitation (P) to annual potential evapotranspiration (PET). A region is considered water-limited if its aridity index is below 0.65, indicating that annual PET substantially exceeds the annual precipitation⁹¹. Conversely, an energy-limited region is defined as an aridity index above 0.65.

Definition of seasonal amplifying and stabilizing LAI trajectories

Amplifying seasonal LAI scenarios were defined as instances where the late-season detrended LAI z-score had a greater positive magnitude than that of the early- and peak-season. Weak stabilization scenarios occurred when both early- and peak-season LAI and late-season LAI had positive detrended z-scores, but the magnitude of the late-season LAI z-score was smaller than that of the early- and peak-season LAI z-score. Strong stabilization scenarios occurred when there was a positive detrended z-score for early- and peak-season LAI but a negative late-season LAI detrended z-score. We performed this same analysis with GPP estimates from 27 flux tower sites and with LAI data from the terrestrial biosphere models in the TRENDY ensemble (multi-model mean).

Statistical analysis

We categorized observed early- and peak-season and late-season LAI detrended zscore into 6×12 bins and calculated the mean probability of each bin occurrence across all grid cells. For early- and peak-season LAI, we grouped LAI zscore into bins: [0, 0.5), [0.5, 1), [1, 1.5), [1.5, 2), [2, 2.5), [2.5, 3], excluding negative LAI zscore during the early- and peak-season. Late-season LAI was divided into twelve zscore bins: [-3, -2.5), [-2.5, -2), [-2, -1.5), [-1.5, -1), [-1, -0.5), [-0.5, 0), [0, 0.5), [0.5, 1), [1, 1.5), [1.5, 2), [2, 2.5), [2.5, 3]. Square brackets [] indicate that the value on that side is included in the bin. For example, [0, 0.5) includes 0 but excludes 0.5. Parentheses () indicate that the value on that side is excluded from the bin. For instance, (0.5, 1) includes 0.5 but excludes 1. This notation ensures clear distinctions between the bins, preventing any overlap between the intervals. We then classified early- and peak-season greenness scenarios as amplifying, weak stabilization, or strong stabilization based on the probability of occurrence in each bin.

We used SEMs to assess how climatic factors and early- and peak-season vegetation LAI legacies (through vegetation-soil feedbacks) influenced late-season LAI for both water-limited regions and energy-

limited regions. SEM is a multivariate statistical approach that synthesizes path, factor, and maximum-likelihood analyses, and provides strong pointers to underlying deterministic processes. Compared with traditional multivariate analyses, SEM allows partitioning the direct and indirect effects that one variable may have on another and is thus useful for exploring complex influence networks in ecosystems. We used the root mean square error of approximation (RMSEA) and a goodness-of-fit index (GFI) and Adjusted Goodness-of-Fit Index (AGFI) to evaluate the fit of the SEM models. The GFI evaluates the proportion of variance in the observed data that is explained by the proposed model. The AGFI is calculated by dividing the GFI by a correction factor based on the number of estimated parameters and the degrees of freedom. Both GFI and AGFI range from 0 to 1, with a value closer to 1 indicating a better fit. The SEM analysis was implemented using the AMOS (version 21.0) software (Amos Development Corporation, Chicago, USA).

Reporting summary

Further information on research design is available in the Nature Portfolio Reporting Summary linked to this article.

Data availability

All data used in this study are stored in a publicly available Zenodo repository (<https://doi.org/10.5281/zenodo.14889969>⁹²). All data supporting the results are available as follows: the MCD15A2H v006 LAI dataset, <https://lpdaac.usgs.gov/products/mod13c1v006/>; The AVHRR LAI3g dataset, <https://drive.google.com/drive/folders/0BwL88nwumpqYaFJmR2poS0d1ZDQ?resourcekey=0-9IRE9s-OtFGfwB5qTpLjZw&usp=sharing>; The FLUXNET2015 dataset, <http://fluxnet.fluxdata.org/data/fluxnet2015-dataset/>; The TRENDY v11 LAI and soil moisture outputs can be accessed from <https://mdosullivan.github.io/GCB/>; The MCD12C1 version 6 vegetation type dataset, <https://lpdaac.usgs.gov/products/mcd12c1v006/>; The CRU TS version 4.05 dataset, https://crudata.uea.ac.uk/cru/data/hrg/cru_ts_4_05/; The root-zone soil moisture from the GLEAM v3.2a data are available at <https://www.gleam.eu/>.

Code availability

All data analyses and modeling were performed using Python 3.10. All code is uploaded github: <https://github.com/zw15772/Seasonal-stabilization-slowed-down-greening>⁹³.

References

- Graven, H. D. et al. Enhanced seasonal exchange of CO₂ by northern ecosystems since 1960. *Science* (1979) **341**, 1085–1089 (2013).
- Wenzel, S., Cox, P. M., Eyring, V. & Friedlingstein, P. Projected land photosynthesis constrained by changes in the seasonal cycle of atmospheric CO₂. *Nature* **538**, 499–501 (2016).
- Parnesan, C. & Yohe, G. A globally coherent fingerprint of climate change impacts across natural systems. *Nature* **421**, 37–42 (2003).
- Cleland, E. E., Chuine, I., Menzel, A., Mooney, H. A. & Schwartz, M. D. Shifting plant phenology in response to global change. *Trends Ecol. Evol.* **22**, 357–365 (2007).
- Lucht, W. et al. Climatic control of the high-latitude vegetation greening trend and Pinatubo effect. *Science* (1979) **296**, 1687–1689 (2002).
- Churkina, G., Schimel, D., Braswell, B. H. & Xiao, X. Spatial analysis of growing season length control over net ecosystem exchange. *Glob. Chang. Biol.* **11**, 1777–1787 (2005).
- Chen, J. M. et al. Vegetation structural change since 1981 significantly enhanced the terrestrial carbon sink. *Nat. Commun.* **10**, 4259 (2019).
- Norby, R. J. et al. Forest response to elevated CO₂ is conserved across a broad range of productivity. *Proc. Natl Acad. Sci.* **102**, 18052–18056 (2005).

9. Walker, A. P. et al. Integrating the evidence for a terrestrial carbon sink caused by increasing atmospheric CO₂. *N. phytologist* **229**, 2413–2445 (2021).
10. Ruehr, S. et al. Evidence and attribution of the enhanced land carbon sink. *Nat. Rev. Earth Environ.* **4**, 518–534 (2023).
11. Piao, S. et al. Characteristics, drivers and feedbacks of global greening. *Nat. Rev. Earth Environ.* **1**, 14–27 (2020).
12. Zhu, Z. et al. Greening of the Earth and its drivers. *Nat. Clim. Chang* **6**, 791–795 (2016).
13. Huang, K. et al. Enhanced peak growth of global vegetation and its key mechanisms. *Nat. Ecol. Evol.* **2**, 1897–1905 (2018).
14. Keenan, T. F. et al. Net carbon uptake has increased through warming-induced changes in temperate forest phenology. *Nat. Clim. Chang* **4**, 598–604 (2014).
15. Angert, A. et al. Drier summers cancel out the CO₂ uptake enhancement induced by warmer springs. *Proc. Natl Acad. Sci.* **102**, 10823–10827 (2005).
16. Dannenberg, M. P., Song, C., Hwang, T. & Wise, E. K. Empirical evidence of El Niño–Southern Oscillation influence on land surface phenology and productivity in the western United States. *Remote Sens Environ.* **159**, 167–180 (2015).
17. Hu, J. I. A., Moore, D. J. P., Burns, S. P. & Monson, R. K. Longer growing seasons lead to less carbon sequestration by a subalpine forest. *Glob. Chang Biol.* **16**, 771–783 (2010).
18. Richardson, A. D. et al. Influence of spring and autumn phenological transitions on forest ecosystem productivity. *Philos. Trans. R. Soc. B: Biol. Sci.* **365**, 3227–3246 (2010).
19. Lian, X. et al. Diminishing carryover benefits of earlier spring vegetation growth. *Nat. Ecol. Evol.* **8**, 218–228 (2024).
20. Lian, X. et al. Seasonal biological carryover dominates northern vegetation growth. *Nat. Commun.* **12**, 983 (2021).
21. Chapin, F. S., Matson, P. A., Mooney, H. A. & Vitousek, P. M. *Principles of Terrestrial Ecosystem Ecology* (Springer, 2002).
22. Liu, Q. et al. Delayed autumn phenology in the Northern Hemisphere is related to change in both climate and spring phenology. *Glob. Chang Biol.* **22**, 3702–3711 (2016).
23. Jump, A. S. et al. Structural overshoot of tree growth with climate variability and the global spectrum of drought-induced forest dieback. *Glob. Chang Biol.* **23**, 3742–3757 (2017).
24. Buermann, W. et al. Widespread seasonal compensation effects of spring warming on northern plant productivity. *Nature* **562**, 110–114 (2018).
25. Zhang, Y., Keenan, T. F. & Zhou, S. Exacerbated drought impacts on global ecosystems due to structural overshoot. *Nat. Ecol. Evol.* **5**, 1490–1498 (2021).
26. Li, Y. et al. Widespread spring phenology effects on drought recovery of Northern Hemisphere ecosystems. *Nat. Clim. Chang* **13**, 182–188 (2023).
27. Wu, C. et al. Increased drought effects on the phenology of autumn leaf senescence. *Nat. Clim. Chang* **12**, 943–949 (2022).
28. Chen, C. et al. China and India lead in greening of the world through land-use management. *Nat. Sustain* **2**, 122–129 (2019).
29. Wang, Z. et al. Large discrepancies of global greening: Indication of multi-source remote sensing data. *Glob. Ecol. Conserv* **34**, e02016 (2022).
30. Myneni, R. B. et al. Global products of vegetation leaf area and fraction absorbed PAR from year one of MODIS data. *Remote Sens Environ.* **83**, 214–231 (2002).
31. Yan, K. et al. Evaluation of MODIS LAI/FPAR product collection 6. Part 2: Validation and intercomparison. *Remote Sens (Basel)* **8**, 460 (2016).
32. Fensholt, R. & Proud, S. R. Evaluation of Earth Observation based global long term vegetation trends—Comparing GIMMS and MODIS global NDVI time series. *Remote Sens Environ.* **119**, 131–147 (2012).
33. Jiang, C. et al. Inconsistencies of interannual variability and trends in long-term satellite leaf area index products. *Glob. Chang Biol.* **23**, 4133–4146 (2017).
34. Yan, K. et al. Evaluation of MODIS LAI/FPAR product collection 6. Part 1: Consistency and improvements. *Remote Sens (Basel)* **8**, 359 (2016).
35. Pastorello, G. et al. The FLUXNET2015 dataset and the ONEFlux processing pipeline for eddy covariance data. *Sci. Data* **7**, 225 (2020).
36. Harris, I., Jones, P., Osborn, T. & Lister, D. Updated high-resolution grids of monthly climatic observations—the CRU TS3.10 Dataset. *Int. J. Climatol.* **34**, 623–642 (2014).
37. Martens, B. et al. GLEAM v3: Satellite-based land evaporation and root-zone soil moisture. *Geosci. Model Dev.* **10**, 1903–1925 (2017).
38. Friedlingstein, P. et al. Global carbon budget 2023. *Earth Syst. Sci. Data* **15**, 5301–5369 (2023).
39. Luo, Y. et al. Evergreen broadleaf greenness and its relationship with leaf flushing, aging, and water fluxes. *Agric Meteorol.* **323**, 109060 (2022).
40. Schimel, D. et al. Observing terrestrial ecosystems and the carbon cycle from space. *Glob. Chang Biol.* **21**, 1762–1776 (2015).
41. Watts, J. D. et al. Carbon uptake in Eurasian boreal forests dominates the high-latitude net ecosystem carbon budget. *Glob. Chang Biol.* **29**, 1870–1889 (2023).
42. Bastos, A. et al. Contrasting effects of CO₂ fertilization, land-use change and warming on seasonal amplitude of Northern Hemisphere CO₂ exchange. *Atmos. Chem. Phys.* **19**, 12361–12375 (2019).
43. Mack, M. C. et al. Carbon loss from boreal forest wildfires offset by increased dominance of deciduous trees. *Science* (1979) **372**, 280–283 (2021).
44. Huxman, T. E. et al. Precipitation pulses and carbon fluxes in semiarid and arid ecosystems. *Oecologia* **141**, 254–268 (2004).
45. Austin, A. T. et al. Water pulses and biogeochemical cycles in arid and semiarid ecosystems. *Oecologia* **141**, 221–235 (2004).
46. Steiner, B. et al. Using phenology to unravel differential soil water use and productivity in a semiarid savanna. *Ecosphere* **15**, e4762 (2024).
47. Currier, C. M. & Sala, O. E. Precipitation versus temperature as phenology controls in drylands. *Ecology* **103**, e3793 (2022).
48. Walker, J. J., De Beurs, K. M. & Wynne, R. H. Dryland vegetation phenology across an elevation gradient in Arizona, USA, investigated with fused MODIS and Landsat data. *Remote Sens Environ.* **144**, 85–97 (2014).
49. Knapp, A. K. et al. Rainfall variability, carbon cycling, and plant species diversity in a mesic grassland. *Science* (1979) **298**, 2202–2205 (2002).
50. Craine, J. M. et al. Timing of climate variability and grassland productivity. *Proc. Natl Acad. Sci.* **109**, 3401–3405 (2012).
51. Craine, J. M. The importance of precipitation timing for grassland productivity. *Plant Ecol.* **214**, 1085–1089 (2013).
52. Barnes, M. L. et al. Vegetation productivity responds to sub-annual climate conditions across semiarid biomes. *Ecosphere* **7**, e01339 (2016).
53. Dermody, O., Weltzin, J. F., Engel, E. C., Allen, P. & Norby, R. J. How do elevated [CO₂], warming, and reduced precipitation interact to affect soil moisture and LAI in an old field ecosystem?. *Plant Soil* **301**, 255–266 (2007).
54. Livensperger, C. et al. Experimentally warmer and drier conditions in an Arctic plant community reveal microclimatic controls on senescence. *Ecosphere* **10**, e02677 (2019).
55. Dow, C. et al. Warm springs alter timing but not total growth of temperate deciduous trees. *Nature* **608**, 552–557 (2022).
56. Fu, Y. S. H. et al. Variation in leaf flushing date influences autumnal senescence and next year’s flushing date in two temperate tree species. *Proc. Natl Acad. Sci.* **111**, 7355–7360 (2014).

57. Keenan, T. F. & Richardson, A. D. The timing of autumn senescence is affected by the timing of spring phenology: implications for predictive models. *Glob. Chang Biol.* **21**, 2634–2641 (2015).
58. Liu, Q. et al. Modeling leaf senescence of deciduous tree species in Europe. *Glob. Chang Biol.* **26**, 4104–4118 (2020).
59. Knowles, J. F., Molotch, N. P., Trujillo, E. & Litvak, M. E. Snowmelt-driven trade-offs between early and late season productivity negatively impact forest carbon uptake during drought. *Geophys Res Lett.* **45**, 3087–3096 (2018).
60. Schimel, J. P. & Bennett, J. Nitrogen mineralization: challenges of a changing paradigm. *Ecology* **85**, 591–602 (2004).
61. Davidson, E. A. & Janssens, I. A. Temperature sensitivity of soil carbon decomposition and feedbacks to climate change. *Nature* **440**, 165–173 (2006).
62. Forkel, M. et al. Enhanced seasonal CO₂ exchange caused by amplified plant productivity in northern ecosystems. *Science* (1979) **351**, 696–699 (2016).
63. Humphrey, V. et al. Sensitivity of atmospheric CO₂ growth rate to observed changes in terrestrial water storage. *Nature* **560**, 628–631 (2018).
64. Wang, S. et al. Recent global decline of CO₂ fertilization effects on vegetation photosynthesis. *Science* (1979) **370**, 1295–1300 (2020).
65. Moore, D. J. P. et al. Annual basal area increment and growth duration of *Pinus taeda* in response to eight years of free-air carbon dioxide enrichment. *Glob. Chang Biol.* **12**, 1367–1377 (2006).
66. Donohue, R. J., Roderick, M. L., McVicar, T. R. & Farquhar, G. D. Impact of CO₂ fertilization on maximum foliage cover across the globe's warm, arid environments. *Geophys Res Lett.* **40**, 3031–3035 (2013).
67. Wang, L. & Fensholt, R. Temporal changes in coupled vegetation phenology and productivity are biome-specific in the Northern Hemisphere. *Remote Sens (Basel)* **9**, 1277 (2017).
68. Chiang, F., Mazdiasni, O. & AghaKouchak, A. Evidence of anthropogenic impacts on global drought frequency, duration, and intensity. *Nat. Commun.* **12**, 2754 (2021).
69. Seneviratne, S. I. et al. *Weather and Climate Extreme Events in a Changing Climate* (Cambridge University Press, 2021).
70. Chen, M., Melaas, E. K., Gray, J. M., Friedl, M. A. & Richardson, A. D. A new seasonal-deciduous spring phenology submodel in the Community Land Model 4.5: Impacts on carbon and water cycling under future climate scenarios. *Glob. Chang Biol.* **22**, 3675–3688 (2016).
71. Murray-Tortarolo, G. et al. Evaluation of land surface models in reproducing satellite-derived LAI over the high-latitude Northern Hemisphere. Part I: Uncoupled DGVMs. *Remote Sens (Basel)* **5**, 4819–4838 (2013).
72. Sitch, S. et al. Recent trends and drivers of regional sources and sinks of carbon dioxide. *Biogeosciences* **12**, 653–679 (2015).
73. Anav, A. et al. Evaluation of land surface models in reproducing satellite Derived leaf area index over the high-latitude northern hemisphere. Part II: Earth system models. *Remote Sens (Basel)* **5**, 3637–3661 (2013).
74. Mahowald, N. et al. Projections of leaf area index in earth system models. *Earth Syst. Dyn.* **7**, 211–229 (2016).
75. CHAPIN, I. I. F. S. Effects of plant traits on ecosystem and regional processes: a conceptual framework for predicting the consequences of global change. *Ann. Bot.* **91**, 455–463 (2003).
76. Hungate, B. A. et al. CO₂ elicits long-term decline in nitrogen fixation. *Science* (1979) **304**, 1291 (2004).
77. Luo, Y. et al. Progressive nitrogen limitation of ecosystem responses to rising atmospheric carbon dioxide. *Bioscience* **54**, 731–739 (2004).
78. Fatichi, S., Pappas, C., Zscheischler, J. & Leuzinger, S. Modelling carbon sources and sinks in terrestrial vegetation. *N. Phytologist* **221**, 652–668 (2019).
79. Paul, M. J. & Foyer, C. H. Sink regulation of photosynthesis. *J. Exp. Bot.* **52**, 1383–1400 (2001).
80. Hudson, A. R., Smith, W. K., Moore, D. J., & Trouet, V. Length of growing season is modulated by Northern Hemisphere jet stream variability. *Int. J. Climatol.* **42**, 5644–5660 (2022).
81. Zhao, T. & Dai, A. The magnitude and causes of global drought changes in the twenty-first century under a low-moderate emissions scenario. *J. Clim.* **28**, 4490–4512 (2015).
82. Holben, B. N. Characteristics of maximum-value composite images from temporal AVHRR data. *Int. J. Remote Sens* **7**, 1417–1434 (1986).
83. Zhu, Z. et al. Global data sets of vegetation leaf area index (LAI) 3g and fraction of photosynthetically active radiation (FPAR) 3g derived from global inventory modeling and mapping studies (GIMMS) normalized difference vegetation index (NDVI3g) for the period 1981 to 2011. *Remote Sens (Basel)* **5**, 927–948 (2013).
84. Pinzon, J. E. & Tucker, C. J. A non-stationary 1981–2012 AVHRR NDVI3g time series. *Remote Sens (Basel)* **6**, 6929–6960 (2014).
85. Loveland, T. R. & Belward, A. S. The IGBP-DIS global 1km land cover data set, DISCover: First results. *Int. J. Remote Sens* **18**, 3289–3295 (1997).
86. Sitch, S. et al. Trends and drivers of regional sources and sinks of carbon dioxide over the past two decades. *Biogeosciences Discuss.* **10**, 20113–20177 (2013).
87. Sulla-Menashe, D., Gray, J. M., Abercrombie, S. P. & Friedl, M. A. Hierarchical mapping of annual global land cover 2001 to present: The MODIS Collection 6 Land Cover product. *Remote Sens Environ.* **222**, 183–194 (2019).
88. Menenti, M., Azzali, S., Verhoef, W. & Van Swol, R. Mapping agroecological zones and time lag in vegetation growth by means of Fourier analysis of time series of NDVI images. *Adv. Space Res.* **13**, 233–237 (1993).
89. Roerink, G. J., Menenti, M. & Verhoef, W. Reconstructing cloudfree NDVI composites using Fourier analysis of time series. *Int. J. Remote Sens* **21**, 1911–1917 (2000).
90. Verhoef, W. Application of harmonic analysis of NDVI time series (HANTS). *Fourier Anal. temporal NDVI South. Afr. Am. Cont.* **108**, 19–24 (1996).
91. Hulme, M. Recent climatic change in the world's drylands. *Geophys Res Lett.* **23**, 61–64 (1996).
92. Zhang W. Seasonal stabilization effects slowed the greening of the Northern Hemisphere over the last two decades. *Zenodo*, <https://doi.org/10.5281/zenodo.14889969> (2025).
93. Zhang W. Seasonal stabilization effects slowed the greening of the Northern Hemisphere over the last two decades. *Github*, <https://doi.org/10.5281/zenodo.15508315> (2025).

Acknowledgements

W.Z., W.K.S. and T.F.K. acknowledge support from NASA Award 80NSSC21K1705. T.F.K. also acknowledges support from the RUBISCO SFA, which is sponsored by the Regional and Global Model Analysis (RGMA) Program in the Climate and Environmental Sciences Division (CESD) of the Office of Biological and Environmental Research (BER) in the U.S. Department of Energy (DOE) Office of Science, and additional support from a DOE Early Career Research Program award #DE-SC0021023 and NASA Award 80NSSC20K1801 and 80NSSC25K7327. M.P.D. acknowledges support from the U.S. National Science Foundation's EPSCoR program (grant 2131853) and NASA award 80NSSC20K1805. J.S.K. acknowledges support from NASA (80NSSC21K1924, 80NSSC22K1238). We also acknowledge Dr. Chi Chen from Rutgers University for their valuable contribution to the AVHRR LAI3g dataset and for the helpful discussions.

Author contributions

W.Z. and D.J.P.M. conceived the study; W.Z., W.K.S., and D.J.P.M. designed the study; W.Z. collected data; W.Z. performed data analysis

and wrote the paper; T.F.K., M.P.D., Y.L., S.W., and J.S.K. contributed the discussion, writing, reviewing and editing.

Competing interests

The authors declare no competing interests.

Additional information

Supplementary information The online version contains supplementary material available at <https://doi.org/10.1038/s41467-025-61308-w>.

Correspondence and requests for materials should be addressed to Wen Zhang or David J. P. Moore.

Peer review information *Nature Communications* thanks Ashley Bal-lantyne and Xu Lian reviewer(s) for their contribution to the peer review of this work. A peer review file is available.

Reprints and permissions information is available at <http://www.nature.com/reprints>

Publisher's note Springer Nature remains neutral with regard to jurisdictional claims in published maps and institutional affiliations.

Open Access This article is licensed under a Creative Commons Attribution-NonCommercial-NoDerivatives 4.0 International License, which permits any non-commercial use, sharing, distribution and reproduction in any medium or format, as long as you give appropriate credit to the original author(s) and the source, provide a link to the Creative Commons licence, and indicate if you modified the licensed material. You do not have permission under this licence to share adapted material derived from this article or parts of it. The images or other third party material in this article are included in the article's Creative Commons licence, unless indicated otherwise in a credit line to the material. If material is not included in the article's Creative Commons licence and your intended use is not permitted by statutory regulation or exceeds the permitted use, you will need to obtain permission directly from the copyright holder. To view a copy of this licence, visit <http://creativecommons.org/licenses/by-nc-nd/4.0/>.

© The Author(s) 2025